Xiangwen Yang, Xiaodong Zhuang, Yinjuan Huang, Jianzhong Jiang, Hao Tian, Dongqing Wu, Fan Zhang, Yiyong Mai, Xinliang Feng

Nitrogen-enriched hierarchically porous carbon materials fabricated by graphene aerogel templated Schiff-base chemistry for high performance electrochemical capacitors

Erstveröffentlichung in / First published in:
Polymer Chemistry. 2015, 6(7), S. 1088–1095 [Zugriff am: 04.11.2019]. Royal Society of Chemistry. ISSN 1759-9962.

DOI: https://doi.org/10.1039/c4py01408a

Polymer Chemistry

PAPER

View Article Online
View Journal | View Issue

Cite this: *Polym. Chem.*, 2015, **6**, 1088

Nitrogen-enriched hierarchically porous carbon materials fabricated by graphene aerogel templated Schiff-base chemistry for high performance electrochemical capacitors†

Xiangwen Yang,[a] Xiaodong Zhuang,[a] Yinjuan Huang,[a] Jianzhong Jiang,[a] Hao Tian,[a] Dongqing Wu,[a] Fan Zhang,[a] Yiyong Mai*[a] and Xinliang Feng*[a,b]

Received 15th October 2014,
Accepted 13th November 2014

DOI: 10.1039/c4py01408a

www.rsc.org/polymers

This article presents a facile and effective approach for synthesizing three-dimensional (3D) graphene-coupled Schiff-base hierarchically porous polymers (GS-HPPs). The method involves the polymerization of melamine and 1,4-phthalaldehyde, yielding Schiff-base porous polymers on the interconnected macroporous frameworks of 3D graphene aerogels. The as-synthesized GS-HPPs possess hierarchically porous structures containing macro-/meso-/micropores, along with large specific surface areas up to 776 $m^2 g^{-1}$ and high nitrogen contents up to 36.8 wt%. Consequently, 3D nitrogen-enriched hierarchically porous carbon (N-HPC) materials with macro-/meso-/micropores were obtained by the pyrolysis of the GS-HPPs at a high temperature of 800 °C under a nitrogen atmosphere. With a hierarchically porous structure, good thermal stability and a high nitrogen-doping content up to 7.2 wt%, the N-HPC samples show a high specific capacitance of 335 F g^{-1} at 0.1 A g^{-1} in 6 M KOH, a good capacitance retention with increasing current density, and an outstanding cycling stability. The superior electrochemical performance means that the N-HPC materials have great potential as electrode materials for supercapacitors.

Introduction

The problems of non-renewable energy and environmental pollution are driving us to efficiently use clean and renewable energy sources. The utilization of renewable energy sources generally requires the support of energy storage devices, such as electrochemical capacitors (ECs).[1–3] Since the performance of ECs is strongly governed by the nature of the electrode materials, the development of electrochemical materials with high activity and desired structures has been the research focus over the past decade. Carbon materials, such as activated carbon, mesoporous carbon, carbon nanotubes and graphene, are the most common and important electrode candidates for ECs.[4–8] In recent years, three-dimensional (3D) electrode materials for ECs based on hierarchically porous carbon with macro-/meso-,[9] meso-/micro-,[10] macro-/micro-,[11] or macro-/meso-/micropores[12] have attracted considerable interest. In these materials, the 3D porous frameworks provide multi-dimensional electron transport pathways. The macropores act as a bulk buffering reservoir for electrolytes to minimize the diffusion distances to the interior surfaces of the pores, the mesopores offer a large accessible surface area for ion transport/charge storage, and the micropores increase the charge accommodation.[9,12]

Monolithic graphene aerogels (GAs) represent a class of new-generation 3D porous carbon materials, which exhibit interconnected macroporous structures, low mass densities, large surface area-to-volume ratios, and high electrical conductivities.[8,9,13–18] Although GAs are devoid of sufficient mesopores and/or micropores, which may improve the efficiency of ion transport/charge storage for ECs, GAs can be used as ideal templates for building up hierarchically porous architectures by integrating mesoporous and/or microporous channels within the interconnected macroporous GA frameworks.[9]

Porous polymers with micro-/mesopores, such as hyper-crosslinked polymers (HCPs),[19] polymers with intrinsic microporosity (PIMs)[20] and covalent organic frameworks (COFs),[21] have recently drawn great attention owing to their porous features, large surface areas and low mass densities along with prominent physical properties and potential applications including energy storage and conversion.[22,23] Among various popular strategies for the synthesis of porous polymers,

[a]*School of Chemistry and Chemical Engineering, Shanghai Jiao Tong University, 800 Dongchuan RD, Shanghai 200240, P. R. China. E-mail: mai@sjtu.edu.cn*
[b]*Department of Chemistry and Food Chemistry Technische, Universitaet Dresden, Mommsenstrasse 4, 01062 Dresden, Germany. E-mail: xinliang.feng@tu-dresden.de*
†Electronic supplementary information (ESI) available: Experimental section, supporting figures and tables. See DOI: 10.1039/c4py01408a

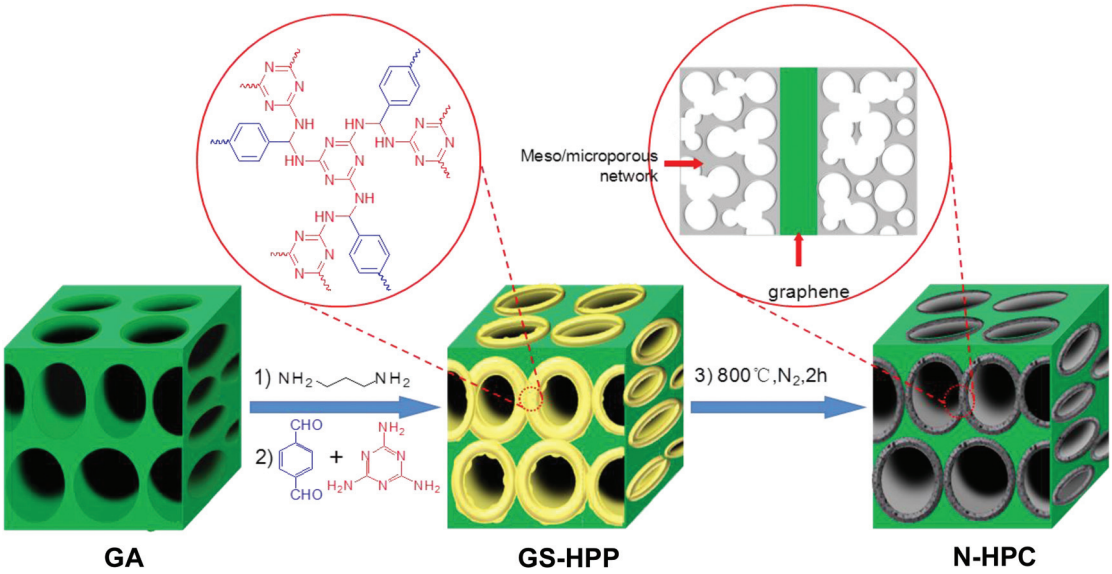

Fig. 1 Schematic illustration of the preparation of 3D nitrogen-enriched hierarchically porous carbon (N-HPC).

Schiff-base chemistry is a facile and "self-correcting" protocol, which does not require any catalyst and may utilize commercially available and inexpensive monomers.[24–28] Moreover, Schiff-base chemistry may introduce nitrogen composition, which can impart the resulting carbon materials with an increased surface area, enhanced electronic conductivity, and improved charge storage efficiency.[26,28]

Apparently, combining the advantages of both GAs and Schiff-base chemistry may provide a possible pathway for the facile synthesis of 3D nitrogen-enriched hierarchically porous polymers. In this regard, we developed a simple and effective approach for synthesizing 3D graphene-coupled Schiff-base hierarchically porous polymers (GS-HPPs) by the polymerization of inexpensive monomers (such as melamine and 1,4-phthalaldehyde) on the interconnected macroporous framework of a GA without employing catalysts (Fig. 1). The resulting GS-HPPs possess a hierarchically porous structure with macropore sizes ranging from hundreds of nanometers to several micrometers, mesopores with 3–50 nm diameters, and micropores with an average size of *ca.* 1 nm. In addition, the incorporation of Schiff-base porous polymers renders the resultant GS-HPPs with large specific surface areas (up to *ca.* 776 $m^2\ g^{-1}$) and high nitrogen contents (up to 36.8 wt%). After thermal treatment at 800 °C under a nitrogen atmosphere, the GS-HPPs were converted into 3D nitrogen-enriched hierarchically porous carbon (N-HPC) structures with macro-/meso-/micropores. To the best of our knowledge, the N-HPC structures represent the first case of the fabrication of hierarchically porous carbon materials by simple GA templated Schiff-base chemistry. The N-HPC structures show good thermal stabilities and possess large specific surface areas and high nitrogen-doping contents (up to 7.2 wt%). As a result, the N-HPC structures exhibit a high specific capacitance up to 335 F g^{-1} at 0.1 A g^{-1} in 6 M KOH electrolyte, a good capacity retention with increasing current density, and an outstanding cycling stability. Such electrochemical performance is superior to those of porous carbon materials prepared from GAs, pyrolyzed porous carbon materials obtained from Schiff-base porous polymers without GA templates, and many reported 3D graphene or nitrogen-doped porous carbon materials.[8,9,29–34]

Results and discussion

The strategy for the synthesis of the 3D GS-HPPs is presented in Fig. 1 and the detail procedures are given in the ESI.† Briefly, monolithic GA was prepared by the hydrothermal assembly of graphene oxide (GO, synthesized by a modified Hummer's method) in an aqueous suspension (1.5 mg mL^{-1}), followed by a freeze-drying process.[9] Then, aminated GA (AGA) was produced by the amidation of the carboxylic acid groups in the GA using 1,3-diaminopropane under catalysis by *N*-hydroxysuccinimide (NHS) and *N*-(3-(dimethylamino)propyl)-*N*′-ethylcarbodiimide hydrochloride (EDC·HCl) in dimethylformamide (DMF) at room temperature for 1 day. After purification, the obtained AGA was immersed in an anhydrous dimethyl sulfoxide (DMSO) solution containing estimated amounts of melamine and 1,4-phthalaldehyde. Then the mixture was incubated at room temperature for 3 days. Next, a condensation reaction between melamine and 1,4-phthalaldehyde on the interconnected macroporous framework of the AGA was carried out under catalyst-free conditions by refluxing the mixture in DMSO under a nitrogen atmosphere for 3 days. The resultant black bulk product was collected and purified by Soxhlet extraction. Finally, the product was filtered and then dried in vacuum at room temperature overnight. The final products are named as GS-HPP-*X* (*i.e.* GS-HPP-5, GS-HPP-10 and GS-HPP-15), where *X* represents the weight percentage of aminated GA in their mixtures with the monomers for polymerization. For comparison, a Schiff-base porous polymer was

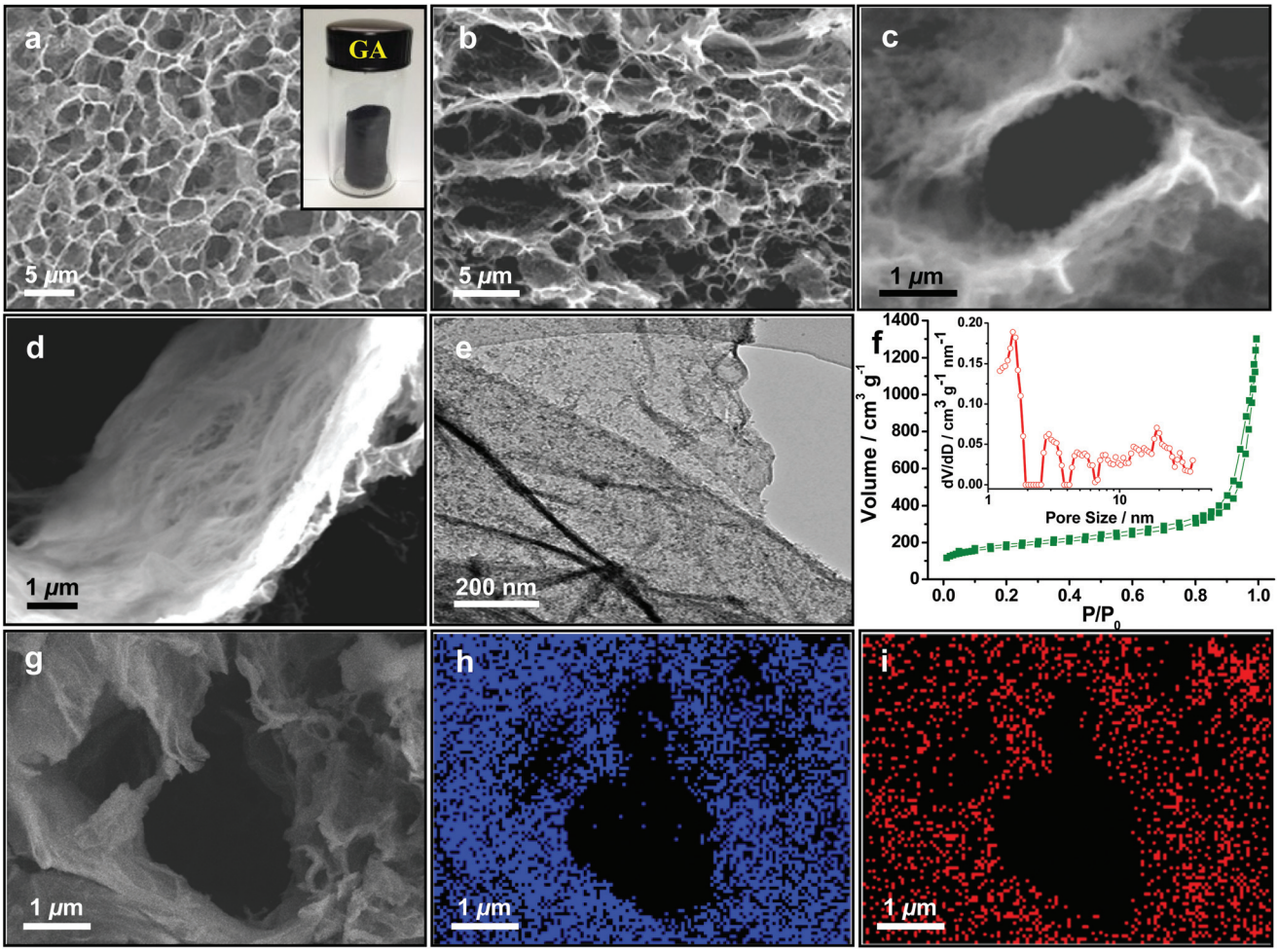

Fig. 2 Morphology and microstructure of the GA and GS-HPP-10. (a) A typical SEM image of the GA with an interconnected macroporous structure. (b) A SEM image of GS-HPP-10, which inherits the interconnected macroporous structure of GA. (c, d) Local-magnification SEM images of GS-HPP-10, in which the homogeneous distribution of Schiff-base polymers can be clearly seen. (e) A representative TEM image of GS-HPP-10. (f) Nitrogen adsorption–desorption isotherm and PSD curve (inset) of GS-HPP-10. (g–i) Typical scanning TEM (STEM) image (g) and the corresponding elemental mapping images of carbon (h) and nitrogen (i) for GS-HPP-10.

synthesized by the polymerization of melamine and 1,4-phthalaldehyde without involving a GA template under similar conditions. The resulting porous polymer is denoted as PP.

The 3D morphology of the resultant monolithic GA (the inset of Fig. 2a) was characterized by scanning electron microscopy (SEM). An interconnected macroporous framework structure is clearly visible in the SEM image (Fig. 2a). The pore sizes range from hundreds of nanometers to several micrometers. Nitrogen adsorption–desorption analysis reveals a typical Brunauer–Emmett–Teller (BET) surface area of 201 $m^2\ g^{-1}$ for the GA (Table 1).

The successful integration of Schiff-base porous polymers on the interconnected macroporous framework of the GA was first verified by Fourier transform infrared (FT-IR) spectroscopy (Fig. S1, ESI†). The bands attributed to the primary amine group of melamine at 3470 and 3420 cm^{-1} (NH_2 stretching) and 1650 cm^{-1} (NH_2 deformation) as well as the bands attributed to the carbonyl group of phthalaldehyde at 2870 cm^{-1} (C–H stretching) and 1690 cm^{-1} (C═O stretching) are absent or attenuated greatly in the spectra of the resulting GS-HPPs. The bands corresponding to the quadrant (1556 cm^{-1}) and semicircle stretching (1479 cm^{-1}) of the triazine ring are present. In addition, some signals originating from the GA (*e.g.* at 3430 cm^{-1} and 1100 cm^{-1}) are also present in the spectra of the GS-HPPs. On the other hand, the elemental analyses reveal high nitrogen contents for the GS-HPPs (36.7 wt%, 30.0 wt% and 24.5 wt% for GS-HPP-5, GS-HPP-10 and GS-HPP-15, respectively, Table 1).

The microstructure of the as-synthesized GS-HPPs was studied by SEM and transmission electron microscopy (TEM). Fig. 2 shows the results obtained from GS-HPP-10 as a typical example, while the results from the other samples are given in the ESI (Fig. S2 and S3†). It can be obviously seen in Fig. 2b that the GS-HPPs inherit the interconnected macroporous framework from the GA, and the pore sizes range from hundreds of nanometers to several micrometers. Furthermore, polymer layers attached uniformly on the macroporous framework can be clearly observed in the high-magnification SEM

Table 1 Physical parameters of the samples discussed in this work

Sample[a]	N^b (wt%)	C^b (wt%)	$S_{BET}{}^c$ [$m^2\ g^{-1}$]	$S_{Langmuir}$ [$m^2\ g^{-1}$]	$V_{Pore}{}^d$ [$cm^3\ g^{-1}$]	$D_{av}{}^e$ [nm]
GA	NA[f]	NA[f]	201	254	0.6	12.4
PP	NA[f]	NA[f]	795	866	2.8	14.4
GS-HPP-5	36.7	42.4	776	977	2.9	15.0
GS-HPP-10	30.0	45.7	631	798	2.0	12.7
GS-HPP-15	24.5	48.2	424	540	1.0	9.6
PC	NA[f]	NA[f]	431	546	0.8	7.2
N-HPC-5	7.2	72.4	436	511	1.1	9.8
N-HPC-10	6.0	77.9	365	424	0.6	6.6
N-HPC-15	4.8	79.1	290	339	0.5	7.9

[a] PP represents the Schiff-base porous polymer from melamine and 1,4-phthalaldehyde; PC represents the porous carbon material prepared by the pyrolysis of PP at 800 °C; GS-HPP-5 represents the graphene-coupled Schiff-base hierarchically porous polymers synthesized using 5 wt% aminated GA during the polymerization (the same principle applies to the definition of GS-HPP-10 and GS-HPP-15); N-HPC-5 represents the nitrogen-enriched hierarchically porous carbon material produced by the pyrolysis of GS-HPP-5 at 800 °C (the same principle applies to the definition of N-HPC-10 and N-HPC-15). [b] Weight content measured by elemental analysis. [c] Surface area calculated from the N_2 adsorption–desorption isotherms using the BET method. [d] Total pore volume at p/p_0 = 0.99. [e] Average pore size based on the adsorption isotherm. [f] NA = not applicable.

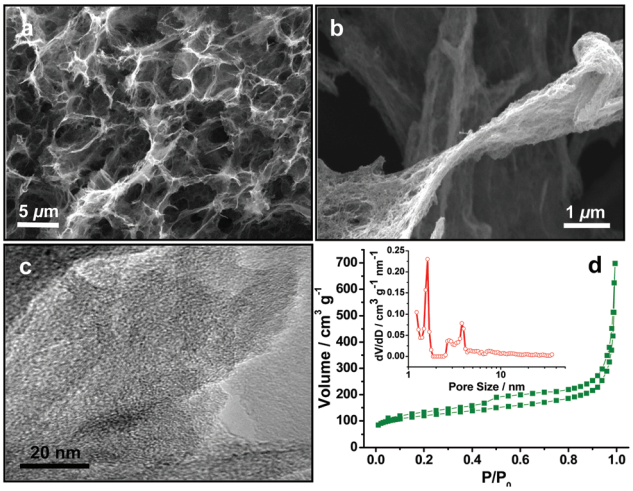

Fig. 3 Microstructural nature of N-HPC-10. (a) A typical SEM image of N-HPC-10, in which the interconnected macroporous framework can be obviously seen. (b) A high-magnification SEM photograph, in which the carbon layers can be clearly observed on the graphene surface. (c) A representative TEM photograph. (d) Nitrogen adsorption–desorption isotherm and PSD curve (inset).

images (Fig. 2c and d), and the incorporation of the polymer layers is further confirmed by TEM observations (Fig. 2e). Elemental mapping images obtained from scanning TEM (STEM) show the homogeneous distribution of carbon and nitrogen in the GS-HPPs (Fig. 2g–i and S4, ESI†). On the other hand, it is known that PP exhibits an amorphous nanoparticle structure (Fig. S5, ESI†).[24,28] In the present work, no free polymer particles or free GA can be seen in the SEM and TEM images. All of the results strongly suggest that the polymerization of melamine and 1,4-phthalaldehyde takes place on the interconnected macroporous framework of the GA.

The hierarchically porous structures of the GS-HPPs were confirmed by nitrogen physisorption measurements. The GS-HPPs exhibited type-IV adsorption–desorption isotherms with a hysteresis loop (Fig. 2f, S2d and S3d†). The isotherms show little uptake at low relative pressures ($P/P_0 < 0.1$), indicating the existence of micropores. A significant hysteresis at high relative pressures ($P/P_0 > 0.1$) can be seen in the isotherms, indicating the abundance of the mesopores. The upward trend at high relative pressures ($P/P_0 > 0.95$) may originate from the presence of macropores.[35,36] In the inset of Fig. 2f, the pore-size distribution (PSD) curve of the GS-HPP-10 sample, calculated from the corresponding adsorption–desorption isotherm, confirms the presence of micropores of *ca.* 0.6 nm and mesopores of 3–50 nm. Similar pore-size distributions were also obtained for the GS-HPP-5 and GS-HPP-15 samples (insets of Fig. S2d and S3d†). Based on the adsorption–desorption isotherms, the specific surface areas, pore volumes and average pore sizes (D_{av}) were calculated and are listed in Table 1. The specific surface areas and pore volumes of the GS-HPPs were up to 776 $m^2\ g^{-1}$ and 2.9 $m^3\ g^{-1}$, respectively, both of which are much higher than the values for GA (*ca.* 201 $m^2\ g^{-1}$ and 0. 6 $m^3\ g^{-1}$) and close to the values for PP (*ca.* 795 $m^2\ g^{-1}$ and 2.8 $m^3\ g^{-1}$).

With hierarchically porous structures and high nitrogen contents, the GS-HPPs can serve as exceptional precursors for template-free pyrolysis, producing 3D nitrogen-enriched hierarchically porous carbon (N-HPC) materials, which have potential application as active electrode materials in supercapacitors.[37] Previous work has demonstrated that 800 °C is an optimum temperature for the pyrolysis of Schiff-base polymers, yielding porous carbon materials with superb performances in electrochemical capacitors.[24,28,38] This temperature was adopted for the carbonization in this work. Thermogravimetric analysis (TGA) revealed that at 800 °C, the GS-HPPs can be converted into N-HPC materials with much higher carbon yields than for PP (for example 24.5 wt% *vs.* 9.1 wt% for GS-HPP-10 *vs.* PP, Fig. S6, ESI†). This indicates the pronounced thermal stability of the GS-HPPs, which is attributed to the presence of graphene.[37]

The SEM images show that the N-HPC materials retain the interconnected macroporous frameworks of the GS-HPPs, and the pore sizes range from hundreds of nanometers to several micrometers (Fig. 3a, S7a and S8a†). In the high-magnification SEM images (Fig. 3b, S7b and S8b†), homogeneous distributions of carbon layers on the surfaces of graphene can be clearly observed. The alternate dark and light areas in the TEM images confirm the presence of porous carbon that is homogeneously decorated on the graphene surface (Fig. 3c, S7c and S8c†). The hierarchically porous nature of the N-HPC materials was confirmed by nitrogen physisorption measurements. All the N-HPC samples showed type-IV adsorption–desorption isotherms (Fig. 3d, S7d and S8d†). The small uptake at low relative pressures ($P/P_0 < 0.1$) indicates the existence of micropores. The H1-type hysteresis loops at high relative pressures

($0.4 < P/P_0 < 0.95$) show that the systems are rich in mesopores. The upward trend at high relative pressures ($P/P_0 > 0.95$) can be attributed to the presence of macropores. Specifically, the pore-size distribution (PSD) curve of the GS-HPP-10 sample, calculated from the corresponding adsorption–desorption isotherm, indicates the presence of micropores of *ca.* 1.6 nm and mesopores of 3–10 nm (inset of Fig. 3d). Similar pore-size distributions were also obtained for the N-HPC-5 and N-HPC-15 samples (insets of Fig. S7d and S8d†). The specific surface areas and pore volumes of these N-HPC samples were up to 436 $m^2\ g^{-1}$ and 1.1 $m^3\ g^{-1}$, respectively (Table 1). Both of these values are much higher than those for GA (201 $m^2\ g^{-1}$ and 0.6 $m^3\ g^{-1}$) and slightly larger than those for PC (431 $m^2\ g^{-1}$ and 0.8 $m^3\ g^{-1}$). The specific surface areas, pore volumes, and D_{av} values of the N-HPC samples are smaller in comparison to those of the corresponding GS-HPP precursors. This is probably due to the degradation of the Schiff-base polymers and the rearrangement of fragments under the carbonization conditions, which might reduce the average pore size and the number of pores in the carbon layers.[37]

The chemical nature of the N-HPC samples was investigated by elemental analysis and X-ray photoelectron spectroscopy (XPS). The elemental analyses indicate that the N-HPC samples obtained after carbonization have high nitrogen doping contents up to 7.2 wt% (Table 1). In order to understand the variation of the different nitrogen species in the N-HPC samples after pyrolysis of the GS-HPPs, the GS-HPP-10 sample was carbonized under an inert atmosphere at 700, 800 and 900 °C. The N1s core-level XPS results reveal high nitrogen contents for the GS-HPP-10 and N-HPC-10 samples prepared at various pyrolysis temperatures (Table S1, ESI†). The nitrogen contents of the GS-HPP-10 sample (36.1 wt%) and N-HPC-10 sample prepared at 800 °C (6.0 wt%) obtained by XPS are in good agreement with those obtained by elemental analysis (30.0 wt% for GS-HPP-10 and 6.0 wt% for N-HPC-10). Moreover, the nitrogen contents of the N-HPC samples decreased as the pyrolysis temperature increased from 700 to 900 °C (Table S1†). Fig. 4 shows the changes in the nitrogen species in the GS-HPPs and N-HPC samples obtained at various pyrolysis temperatures. Before pyrolysis, the GS-HPPs possess three types of nitrogen components, which can be assigned to the 1,3,5-triazine units (C–N=C) at ~398.0 eV, the primary amine ($C–NH_2$) at ~398.6 eV, and the secondary amine (C–NH–C) moieties at ~399.2 eV before pyrolysis.[28] After thermal treatment, the nitrogen species were transformed to pyridine nitrogen (~398.3 eV) and graphitic nitrogen (~401.0 eV).[28] Obviously, the ratio of pyridine N to graphitic N (Table S1†) for the N-HPC samples decreases as the pyrolysis temperature increases, indicating a better thermal stability of graphitic nitrogen compared to pyridinic nitrogen.

The N-HPC materials with a hierarchically porous structure and a high nitrogen doping content hold promise for applications in electrochemical capacitors. To evaluate the performance of the N-HPC samples as electrodes for supercapacitors, the electrochemical performances of the N-HPC samples were examined under alkaline conditions (6 M KOH aqueous solution) using a conventional cell with a three-electrode configuration. Typically, the cyclic voltammetry (CV) curves of the N-HPC samples measured at a scan rate of 5 mV s^{-1} exhibited typical electrical double layer behavior with high capacitance values (Fig. S9, ESI†). Notably, the current density of the N-HPC-10 sample is higher than the densities of the other N-HPC samples and PC, indicating a higher specific capacitance for N-HPC-10. The capacitive performance was further studied by galvanostatic charge/discharge measurements (Fig. 5a and b). The nearly triangular charge/discharge curves at different current densities indicate a nearly ideal electrical double layer capacitive behavior and efficient ion transport throughout the N-HPC-10 electrodes (Fig. 5a). According to the discharge curve, the specific capacitance of N-HPC-10 is calculated to be 335 F g^{-1} at 0.1 A g^{-1}, which is superior to N-HPC-5 (288 F g^{-1}), N-HPC-15 (192 F g^{-1}), PC (227 F g^{-1}) and GA (187 F g^{-1}). It should be emphasized that the specific capacitance of N-HPC-10 is better than the specific capacitance of many reported heteroatom-doped porous carbon materials with much larger specific surface areas but without macropores, such as N-doped porous carbon (298 F g^{-1}, S_{BET} = 1724 $m^2\ g^{-1}$),[29] B/N-co-doped porous carbon (268 F g^{-1}, S_{BET} = 894 $m^2\ g^{-1}$),[30] and KOH-activated nitrogen-doped porous carbon (259 F g^{-1}, S_{BET} = 2970 $m^2\ g^{-1}$).[31] The capacitance of N-HPC-10 is also higher than the capacitance of many reported graphene-based porous carbon materials, including reduced

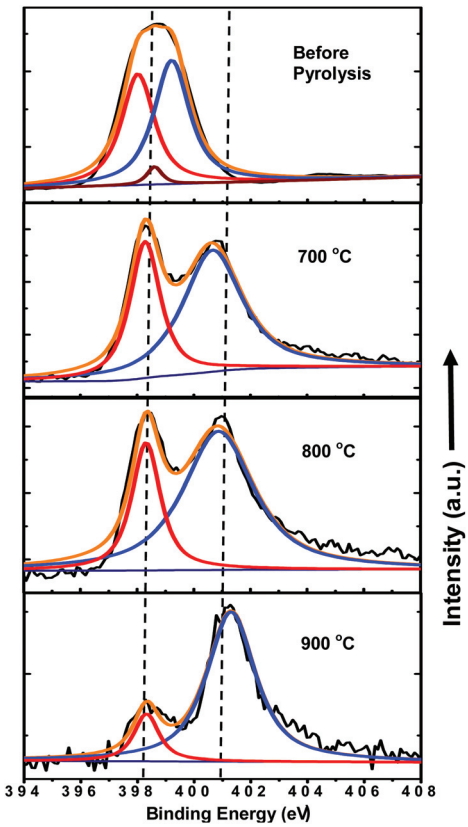

Fig. 4 N1s core-level spectra for GS-HPP-10 and N-HPC-10 prepared under different pyrolysis temperatures.

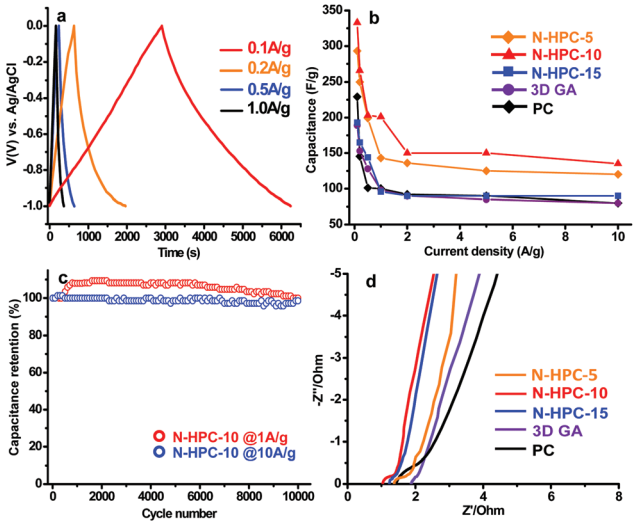

Fig. 5 Electrochemical performance of the N-HPC samples, PC and GA as electrodes for supercapacitors. (a) Galvanostatic charge/discharge curves for N-HPC-10 at different current densities in 6 M KOH electrolyte. (b) Capacitance retention for the N-HPC samples, PC and GA with increasing current density. (c) Cycling stability of N-HPC-10 evaluated at low and high current densities. (d) Nyquist plots for the N-HPC samples, PC and GA under open-circuit voltage.

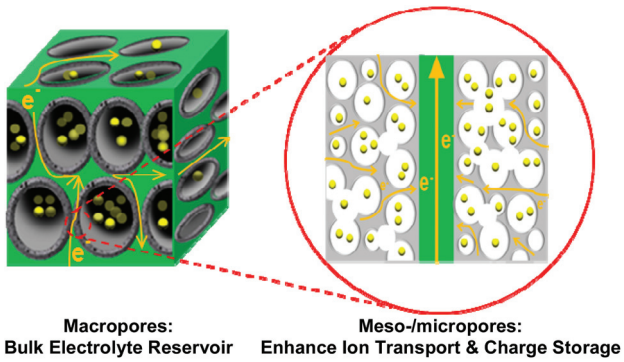

Fig. 6 Illustration of the roles of macropores and meso-/micropores in the 3D hierarchically porous frameworks of the N-HPC samples for electrochemical capacitors.

GO foams (110 F g^{-1}),[8] 3D GA-based mesoporous carbon (226 F g^{-1}),[9] graphene-based mesoporous carbon nanosheets without macropores (148 F g^{-1}),[9] hydrazine reduced graphene hydrogels (220 F g^{-1}),[32] nitrogen-doped graphene hydrogels (190 F g^{-1}),[33] hierarchically porous carbon prepared from melamine resin functionalized GO (210 F g^{-1}),[34] *etc*.

The N-HPC-10 sample also displays a good capacitance retention (Fig. 5b). A high specific capacitance of ~150 F g^{-1} was obtained for N-HPC-10 at a current density of 2.0 A g^{-1}, and this capacitance value remained stable with increasing current densities (up to 10 A g^{-1} in our experiment). The other two N-HPC samples, GA and PC exhibited similar capacitance retention behavior, however, their specific capacitance values are much lower than the value for N-HPC-10 over the whole current density window (Fig. 5b). The cycling stability of N-HPC-10 was further evaluated by galvanostatic charge–discharge measurements at 1.0 and 10 A g^{-1} in a 6 M KOH aqueous solution. Remarkably, almost no capacitance loss was observed for N-HPC-10 after 10 000 cycles at both low and high current densities (Fig. 5c). The capacity was even enhanced by about 10% after 1000 cycles at the low current density of 1.0 A g^{-1}. This increase may be attributed to an improvement in the ion accessibility in the 3D graphene frameworks during the cycling process, which leads to increased accommodation for the charges.[9,12]

In order to understand the superior capacitor performance of N-HPC-10, the conductivity differences between N-HPC-10 and the other samples were examined. The impedance spectra are shown in Fig. 5d. The semicircle in the impedance curve for N-HPC-10 was found to be smaller than for the other samples, indicating a smaller charge-transfer resistance for N-HPC-10. According to the equivalent circuit, the charge-transfer resistance of N-HPC-10 is ~0.3 Ω, which is smaller than the values for N-HPC-5, N-HPC-15, GA and PC (Fig. S10 and the caption, ESI†). A lowering in the charge-transfer resistance is critical for increasing the specific power output of supercapacitors.[39,40]

The excellent electrochemical performance of N-HPC-10 is considered to arise from its nitrogen-enriched hierarchically porous structure, which provides a synergistic effect of macro- and meso-/micropores (Fig. 6). First, the interconnected macropores may buffer ions and thus shorten the diffusion distances from the external electrolyte to the interior surfaces. Second, the meso-/micropores in the thin walls, along with the presence of micropores derived from the stacked graphene layers, can enhance ion transport and charge storage. Third, the conductive graphene sheets which construct the 3D frameworks may serve as multidimensional pathways to facilitate the transport of electrons in the bulk electrode. Among the N-HPC samples, N-HPC-10 shows a better capacitor performance compared to N-HPC-5. This is probably due to the higher content of graphene in N-HPC-10, which may provide better electronic conductivity and thermal stability properties.[8,9] N-HPC-5 exhibits a better capacitor performance than N-HPC-15 owing to the higher surface area and nitrogen doping content, which may render more active sites for ion transport and charge storage.

Conclusions

In this work, we synthesized 3D GS-HPPs *via* the polymerization of melamine and 1,4-phthalaldehyde, producing Schiff-base micro-/mesoporous polymers within the interconnected macroporous graphene frameworks. The resultant GS-HPPs possessed large specific surface areas up to 776 m^2 g^{-1} and high nitrogen contents up to 36.8 wt%. 3D N-HPC materials were then fabricated by the pyrolysis of the GS-HPPs at 800 °C under a nitrogen atmosphere. The N-HPC samples possessed

hierarchically porous structures containing macro-/meso-/micropores, good thermal stabilities and high nitrogen-doping contents up to 7.2 wt%. In particular, the N-HPC-10 sample, fabricated by the pyrolysis of GS-HPP-10 with *ca.* 10 wt% graphene, showed a high specific capacitance of 335 F g^{-1} at 0.1 A g^{-1} in 6 M KOH with good capacitance retention as well as superior cycling stability with no capacitance loss after 10 000 cycles. Considering the outstanding performance and the facile synthesis approach *via* GA templated Schiff-base chemistry, the N-HPC samples containing macro-/meso-/micropores hold promise for application as electrode materials in electrochemical capacitors. Moreover, we believe that the method developed in this work is promising for building up a wide range of other different types of hierarchically porous carbon materials. For instance, the GS-HPPs are an ideal template for the fabrication of hierarchically porous carbon/metal oxide hybrids *via* the incorporation of metal oxide nanoparticles, such as Fe_3O_4 or Co_3O_4, by taking advantage of the affinity of the corresponding metal ion and the nitrogen atoms in the GS-HPPs. Employing monomers containing other heteroatoms (such as boron or sulphur) can produce the corresponding heteroatom-doped hierarchically porous carbon materials. These materials are expected to have potential applications in *e.g.* supercapacitors, lithium-ion batteries and fuel cells.

Acknowledgements

The authors appreciate the financial support from 973 Programs of China (2012CB933404, 2013CB328804, 2013CBA01602 and 2014CB239701), Natural Science Foundation of China (21320102006 and 21304057), Natural Science Foundation of Shanghai City (13ZR1421200), Program for Professor of Special Appointment in Shanghai City (Eastern Scholar), and Ph.D. Programs Foundation of Ministry of Education of China for Young Scholars (20130073120088). We also thank the Instrumental Analysis Center of Shanghai Jiao Tong University for some measurements.

References

1 Y. Sun, Q. Wu and G. Shi, *Energy Environ. Sci.*, 2011, **4**, 1113.
2 S. Yang, R. E. Bachman, X. Feng and K. Müllen, *Acc. Chem. Res.*, 2013, **46**, 116.
3 Y. Mai, F. Zhang and X. Feng, *Nanoscale*, 2014, **6**, 106.
4 D. W. Wang, F. Li, M. Liu, G. Q. Lu and H. M. Cheng, *Angew. Chem., Int. Ed.*, 2008, **47**, 373.
5 Y. W. Zhu, S. Murali, M. D. Stoller, K. J. Ganesh, W. W. Cai, P. J. Ferreira, A. Pirkle, R. M. Wallace, K. A. Cychosz, M. Thommes, D. Su, E. A. Stach and R. S. Ruoff, *Science*, 2011, **332**, 1537.
6 V. Presser, M. Heon and Y. Gogotsi, *Adv. Funct. Mater.*, 2011, **21**, 810.
7 Y. Zhai, Y. Dou, D. Zhao, P. Fulvio, R. Mayes and S. Dai, *Adv. Mater.*, 2011, **23**, 4828.
8 Z. Niu, J. Chen, H. H. Hng, J. Ma and X. Chen, *Adv. Mater.*, 2012, **24**, 4144.
9 Z. Wu, Y. Sun, Y. Tan, S. Yang, X. Feng and K. Müllen, *J. Am. Chem. Soc.*, 2012, **134**, 19532.
10 M. Rose, Y. Korenblit, E. Kockrick, L. Borchardt, M. Oschatz, S. Kaskel and G. Yushin, *Small*, 2011, **7**, 1108.
11 M. C. Gutierrez, F. Pico, F. Rubio, J. M. Amarilla, F. J. Palomares, M. L. Ferrer, F. del Monte and J. M. Rojo, *J. Mater. Chem.*, 2009, **19**, 1236.
12 H. Jiang, J. Ma and C. Li, *Adv. Mater.*, 2012, **24**, 4197.
13 Z. Tang, S. Shen, J. Zhuang and X. Wang, *Angew. Chem., Int. Ed.*, 2010, **49**, 4603.
14 Z. Chen, W. Ren, L. Gao, B. Liu, S. Pei and H. Cheng, *Nat. Mater.*, 2011, **10**, 424.
15 K. S. Novoselov, V. I. Fal'ko, L. Colombo, P. R. Gellert, M. G. Schwab and K. Kim, *Nature*, 2012, **490**, 192.
16 X. Huang, K. Qian, J. Yang, J. Zhang, L. Li, C. Yu and D. Zhao, *Adv. Mater.*, 2012, **24**, 4419.
17 Y. Zhao, C. Hu, Y. Hu, H. Cheng, G. Shi and L. Qu, *Angew. Chem., Int. Ed.*, 2012, **51**, 11371.
18 H. Cong, X. Ren, P. Wang and S. Yu, *ACS Nano*, 2012, **6**, 2693.
19 Y. Luo, B. Li, W. Wang, K. Wu and B. Tan, *Adv. Mater.*, 2012, **24**, 5703.
20 J. Weber and A. Thomas, *J. Am. Chem. Soc.*, 2008, **130**, 6334.
21 P. Kuhn, M. Antonietti and A. Thomas, *Angew. Chem., Int. Ed.*, 2008, **47**, 3450.
22 D. Wu, F. Xu, B. Sun, R. Fu, H. He and K. Matyjaszewski, *Chem. Rev.*, 2012, **112**, 3959.
23 X. Feng, X. Ding and D. Jiang, *Chem. Soc. Rev.*, 2012, **41**, 6010.
24 H. W. Spiess, A. Thomas, X. Feng and K. Müllen, *J. Am. Chem. Soc.*, 2009, **131**, 7216.
25 F. J. Uribe-Romo, C. J. Doonan, H. Furukawa, K. Oisaki and O. M. Yaghi, *J. Am. Chem. Soc.*, 2011, **133**, 11478.
26 R. Chakrabarty, P. S. Mukherjee and P. J. Stang, *Chem. Rev.*, 2011, **111**, 6810.
27 E. Preis, C. Widling, G. Brunklaus, J. Schmidt, A. Thomas and U. Scherf, *ACS Macro Lett.*, 2013, **2**, 380.
28 X. Zhuang, F. Zhang, D. Wu and X. Feng, *Adv. Mater.*, 2014, **26**, 3081.
29 L. Hao, B. Luo, X. Li, M. Jin, Y. Fang, Z. Tang, Y. Jia, M. Liang, A. Thomas, J. Yang and L. Zhi, *Energy Environ. Sci.*, 2012, **5**, 9747.
30 H. Guo and Q. Gao, *J. Power Sources*, 2009, **186**, 551.
31 H. Wang, Q. Gao and J. Hu, *Microporous Mesoporous Mater.*, 2010, **131**, 89.
32 L. Zhang and G. Shi, *J. Phys. Chem. C*, 2011, **115**, 17206.

33 P. Chen, J. Yang, S. Li, Z. Wang, T. Xiao, Y. Qian and S. Yu, *Nano Energy*, 2013, **2**, 249.
34 J. H. Lee, N. Park, B. G. Kim, D. S. Jung, K. Im, J. Hur and J. W. Choi, *ACS Nano*, 2013, **7**, 9366.
35 U. H. F. Bunz, K. Seehafer, F. L. Geyer, M. Bender, I. Braun, E. Smarsly and J. Freudenberg, *Macromol. Rapid Commun.*, 2014, **35**, 1466.
36 X. Li, S. Yang, J. Sun, P. He, X. Xu and G. Ding, *Carbon*, 2014, **78**, 38.
37 L. Lai, H. Yang, L. Wang, B. K. Teh, J. Zhong, H. Chou, L. Chen, W. Chen, Z. Shen, R. S. Ruoff and J. Lin, *ACS Nano*, 2012, **6**, 5941.
38 X. Zhuang, F. Zhang, D. Wu, N. Forler, H. Liang, M. Wagner, D. Gehrig, M. R. Hansen, F. Laquai and X. Feng, *Angew. Chem., Int. Ed.*, 2013, **52**, 9668.
39 L. Yang, S. Cheng, Y. Ding, X. Zhu, Z. Wang and M. Liu, *Nano Lett.*, 2012, **12**, 321.
40 L. Hao, X. Li and L. Zhi, *Adv. Mater.*, 2013, **25**, 3899.